

## Experiment 27

### THE NORMAL (CLASSICAL) ZEEMAN EFFECT

INTRODUCTION	1
THEORY	2
Generation of light by charged particle motion	2
An isotropic, hot gas and unpolarized light emission	4
Breaking the symmetry of the gas by applying a magnetic field	5
Harmonic oscillator with an applied magnetic field	6
Consequences of the analysis for experimental measurements	7
THE APPARATUS	9
Fabry-Pérot interferometer	9
Viewing Zeeman splitting	13
Hall probe	15
PROCEDURE	16
Calibration and Alignment	16
Hall probe	16
Fabry-Pérot etalon	16
Spectrometer adjustments and line identification	18
Data acquisition	18
Investigation of line polarizations	19
Securing the apparatus	19
ANALYSIS	19
PRELAB PROBLEMS	20
REFERENCES	22
APPENDIX A: QUANTUM THEORY OF ZEEMAN SPLITTING	
Angular momentum and magnetic moment of a single atomic electron	A-1
Multiple-electron atoms; g-factor	A-3
Spectroscopic term notation	A-6
Racah's JI coupling scheme for excited atomic states	A-7
Electric dipole radiation selection rules and Zeeman splitting	A-8
Normal Zeeman lines of neon	A-10



## THE NORMAL (CLASSICAL) ZEEMAN EFFECT

### INTRODUCTION

Spectroscopy was a well-established discipline by the latter half of the 19<sup>th</sup> century. Investigators had cataloged the visible-light spectra of many elements and compounds, both from laboratory experiments and from the observation of spectra from the sun and other astronomical bodies.<sup>1</sup> An emission spectrum of hot neon gas, for example, is shown in Figure 1.

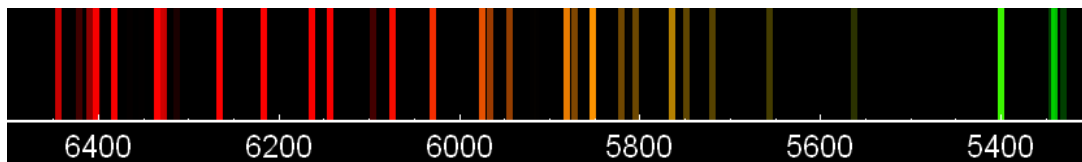


**Figure 1: A portion of the visible-light emission spectrum of neutral neon gas, which you will use for this experiment (wavelengths are in angstroms). This plot is similar to how the neon spectrum might appear through a low-resolution, prism spectroscope. It was generated from NIST atomic line data available at <http://www.nist.gov/pml/data/asd.cfm>.**

Although it was assumed by many physicists that such spectra must originate from the oscillatory motion of electric charge within the atoms or molecules of a material, even a rudimentary theory of the fundamental processes within atoms by which light may be generated or absorbed was yet to be developed. During 1896–1897 Pieter Zeeman, the outstanding Dutch experimental physicist, observed the splitting of the spectral lines of both sodium and cadmium atoms in the presence of a strong magnetic field.<sup>2</sup> Efforts by Zeeman and his colleague, the eminent theoretical physicist Hendrik Lorentz, determined that this splitting could be explained by oscillations of the electron—the first-to-be-identified elementary particle, newly-discovered by J. J. Thompson in 1897.<sup>3</sup> This identification of atomic spectral lines with oscillations of electrons within atoms earned Zeeman and Lorentz the 1902 Nobel Prize in physics (only the second time the Nobel had been awarded); J. J. Thompson in turn won the 1906 prize for his work.

<sup>1</sup> For instance, spectral lines of helium were first discovered in the solar spectrum by the French astronomer Jules Janssen during a total solar eclipse in 1868. Helium was not identified from an earthly source until 1895 by Swedish chemists Cleve and Langlet.

<sup>2</sup> Pieter Zeeman had just been awarded his Ph.D. in 1893 at Leyden University. To make his seminal observations, he used a Tesla-level field and an original, 10 foot radius *Rowland diffraction grating* with approximately 590 lines/mm. He was evidently inspired by an unsuccessful experimental attempt by Michael Faraday (Kox, 1997).

<sup>3</sup> Electrons were identified by investigating cathode rays, first observed variously by J. Hittorf, E. Goldstein, W. Crookes, and A. Schuster during the period 1869–1890. In 1896 J. J. Thompson definitively identified these “rays” as consisting of identical, previously unidentified, negatively-charged particles with a charge/mass ratio over 1800 times larger than that of a positively-charged Hydrogen ion (a proton, as we now know it). His 1897 paper established him as the “discoverer” of the electron, whose name was actually coined by G. Stoney in 1891 as the “fundamental unit quantity of electricity.”

In this experiment you will examine the effects of a magnetic field on the wavelengths of the spectral lines of neon. By familiarizing yourself with Lorentz's simple and elegant but powerful argument, you can predict the polarizations of the emitted spectral lines and use the observed splitting of the lines to determine an accurate estimate of the electron's charge/mass ratio,  $q_e/m_e = -e/m_e$ .<sup>4</sup> However, you will discover that Lorentz's theory describes the behaviors of only a tiny fraction of the spectral lines you observe, implying that the dynamics of the electrons within an atom require additional physics unknown to Lorentz (or, indeed, that are explainable by any classical theory of charged particle interactions with an electromagnetic field).

## THEORY

### *Generation of light by charged particle motion*

Before proceeding with our derivation of Lorentz's classical theory of the Zeeman Effect, we must briefly review (or introduce) how electromagnetic radiation may be generated by the classical motion of charged particles such as an electron.<sup>5</sup> Assume we sit at the origin of our coordinate system, and we ask what would be the electric field  $\vec{E}(t)$  and magnetic field  $\vec{B}(t)$  produced here (position =  $\mathbf{0}$ ) by a charge  $q$  following a path  $\vec{r}(t)$  through space. *Feynman's* equations (28.3) and (28.4) give our equations (27.1) and (27.2):

$$\vec{E}(t) = \frac{-q}{4\pi\epsilon_0} \left[ \frac{\hat{\mathbf{r}}(t_{ret})}{r^2(t_{ret})} + \frac{r(t_{ret})}{c} \frac{d}{dt} \left( \frac{\hat{\mathbf{r}}(t_{ret})}{r^2(t_{ret})} \right) + \frac{1}{c^2} \frac{d^2}{dt^2} \hat{\mathbf{r}}(t_{ret}) \right] \quad (27.1)$$

$$\vec{B}(t) = -\hat{\mathbf{r}}(t_{ret}) \times \frac{1}{c} \vec{E}(t) \quad (27.2)$$

where the *retarded time*  $t_{ret}$  refers to the time at which light (electromagnetic radiation) would have had to leave the source charge  $q$  in time to arrive at our position (the origin) at time  $t$ , that is  $t_{ret} = t - r/c$ , where  $r$  was the distance of the charge when the light would have been emitted:  $r = r(t_{ret})$ . The unit vector  $\hat{\mathbf{r}}(t_{ret})$  points in the direction of the charge at that earlier time, i.e. the *apparent* direction to the charge at our time  $t$ . Note that all of the positions referred to in (27.1) and (27.2) must be evaluated at the retarded time  $t_{ret}$ . As explained in *Feynman*, the first two terms in the equation for  $\vec{E}(t)$  simply represent the “effective” inverse square law Coulomb field produced at the observer's position by the moving charge, and thus do not really contribute to the production of electromagnetic radiation by the charge; it is the third and final term in (27.1) which interests us.

Assume that the charge  $q$  is constrained to orbit about some fixed point  $\mathbf{R}$  by a “Hook's law” force  $\vec{F} = -m\omega_0^2 \vec{x}$ , where  $m$  is the particle's mass and  $\vec{x}$  is its position relative to its equilibrium

<sup>4</sup> We take  $e$  to be the absolute value of the electron's charge, so  $q_e = -e$ .

<sup>5</sup> As with most of the ideas introduced in this course, Feynman explains it very clearly and elegantly. See his *Lectures on Physics*, Volume I chapter 28 (Feynman, Leighton, & Sands, 1964, 2006). Our presentation follows his (we refer to this text as *Feynman*).

position  $\mathbf{R}$ . The motion of the charge about  $\mathbf{R}$  would then be simple-harmonic with angular frequency  $\omega_0$ , its path describing some ellipse centered on  $\mathbf{R}$ . If the maximum amplitude of the charge's motion away from  $\mathbf{R}$  is very small compared to the distance of  $\mathbf{R}$  away from the origin (our point of observation), then the tip of the unit vector  $\hat{\mathbf{r}}$  toward the charge will in turn sweep out a very small ellipse in a plane perpendicular to the line of sight from the origin toward  $\mathbf{R}$ . In addition, to a very good approximation the retarded time will be given by  $t_{ret} = t - R/c$ , where  $R$  is the fixed distance to the motion's center  $\mathbf{R}$ . Thus the tip of the unit vector  $\hat{\mathbf{r}}(t_{ret}) = \hat{\mathbf{r}}(t - R/c)$  will also undergo simple-harmonic motion at the same frequency  $\omega_0$ , describing an ellipse about the line of sight toward  $\mathbf{R}$ . The shape of the ellipse  $\hat{\mathbf{r}}$  traces will be the projection of the charge's orbital ellipse onto a plane perpendicular to the line of sight toward  $\mathbf{R}$  (see Figure 2).

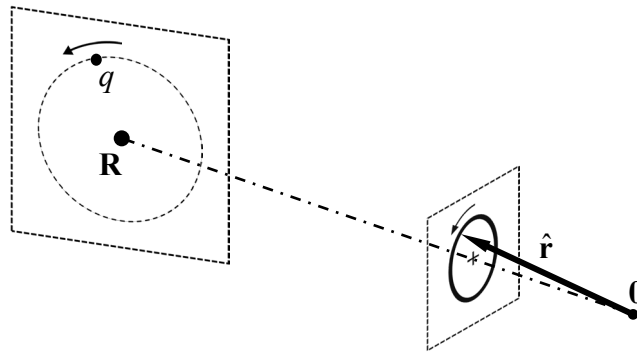


**Figure 2: Simple-harmonic motion of a charge  $q$  about its equilibrium position  $\mathbf{R}$  follows an elliptical path in some plane. The projection of this orbit onto a transverse plane as seen by an observer at  $\mathbf{O}$  also traces out an elliptical path, which is the path followed by the tip of the unit vector  $\hat{\mathbf{r}}$  as it traces out the apparent direction toward the charge  $q$ . Clearly, the period of  $q$ 's orbit around  $\mathbf{R}$  is the same as that of the tip of  $\hat{\mathbf{r}}$  around the line of sight toward  $\mathbf{R}$ .**

Orienting the  $z$ -axis along the line of sight toward  $\mathbf{R}$  and the  $x$  and  $y$  axes along the major and minor axes of the ellipse traced out by the tip of  $\hat{\mathbf{r}}$ , and with a suitable choice for  $t = 0$ , the motion of  $\hat{\mathbf{r}}$  becomes

$$\hat{\mathbf{r}}(t) = \hat{z} + \hat{x} a \cos \omega_0 t + \hat{y} b \sin \omega_0 t \quad (27.3)$$

where  $a$  and  $b$  are each  $\ll 1$ , and they are each  $\propto R^{-1}$  as the distance  $R$  between the observer and  $\mathbf{R}$  varies. Using the third term only of (27.1),

$$\vec{E}(t) = \frac{q}{4\pi\epsilon_0} \frac{\omega_0^2}{c^2} (\hat{x} a \cos \omega_0 t + \hat{y} b \sin \omega_0 t) \quad (27.4)$$

Thus in general the electric field  $\vec{E}(t)$  at the observer's location traces out an elliptical path in a plane transverse to the line of sight toward the charge, and its amplitude varies as  $R^{-1}$ . This oscillation corresponds, naturally, to *elliptically-polarized light* with angular frequency  $\omega_0$  propagating away from the charge toward the observer. *The polarization of the light and its amplitude are determined by the apparent transverse motion of the charge as seen by the observer.* The intensity of the light goes as  $E^2 \propto a^2 + b^2 \propto R^{-2}$ , so each component of the

polarization contributes independently to the light's intensity, and the intensity follows an inverse-square law. Light generated in this manner from an oscillating charge is generally referred to as *electric dipole radiation*. If one of the amplitudes  $a$  or  $b$  vanishes (so that the apparent transverse motion of the charge is along a straight line) then the resulting polarization is linear. If both  $a$  and  $b$  vanish (the apparent motion of the charge is directly along the observer's line of sight), then no electromagnetic radiation is generated in the direction toward the observer. Note that this has been a classical derivation based on a charge following a continuous, well-defined path and using Maxwell's equations.

### ***An isotropic, hot gas and unpolarized light emission***

The emission spectrum of a monatomic gas such as neon consists of a set of very narrow spectral lines with well-defined wavelengths (the line widths are greatly exaggerated in Figure 1). Typically, an atomic spectral line width is  $\sim 10^{-6}$  to  $10^{-7}$  of the line's wavelength. Additionally, the charge motion which generates a particular line must be very accurately simple-harmonic, because no *overtones* (additional lines at multiples of the fundamental frequency) are observed in a typical atomic spectrum.<sup>6</sup> These facts imply that the emission of a particular spectral line wavelength from a particular atom will result in a long wave-train with a well-defined frequency and polarization as seen by an observer (typically  $\sim 10^{-8}$  sec duration with oscillations at several  $\times 10^{14}$  Hz). The polarization will depend on the relative orientation of the atomic charge oscillation to the direction toward the observer, as explained in the previous section (Figure 2).

A hot gas of a macroscopic number of atoms, if no external forces are applied, will be on average completely homogeneous and isotropic as the individual atoms fly about randomly with thermal velocities, frequently colliding with each other and with the walls of their container (of course, at any instant there will be slight, constantly changing inhomogeneities and anisotropies in the neighborhood of any particular atom). This implies that the orientations of the simple-harmonic orbits of the charges in the various atoms associated with the emission of a particular spectral line will be distributed completely randomly and uniformly in angle and possibly elongation (ellipticity). For a particular observer, the polarization of the spectral line's radiation from any particular atom will be randomly determined but well-defined, whereas the next atom to emit will have a completely unrelated polarization. Consequently, although the observed polarization will remain well-defined for periods of up to a million cycles or so, over the long term it will vary in a completely unpredictable way. This is what is meant by the phrase *unpolarized radiation* at a particular wavelength.

---

<sup>6</sup> This was pointed out by Robert Leighton in chapter 2 of his outstanding book *Principles of Modern Physics* (Leighton, 1959) (unfortunately out of print, but the lab has a few copies). The analysis provided here is partly based on his text, which we refer to as *Leighton*.

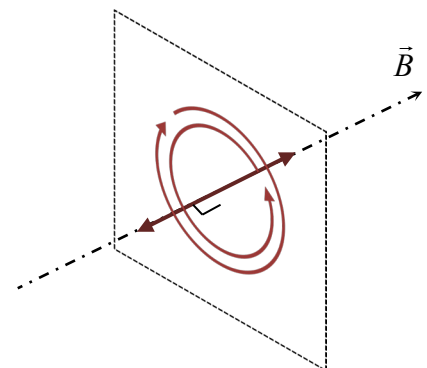
### ***Breaking the symmetry of the gas by applying a magnetic field***

Because the interior of the hot gas described above is isotropic (on average), it displays maximal directional symmetry: it is spherically symmetric and thus all directions are equivalent. When a constant, uniform magnetic field is then applied to the hot gas, this maximal symmetry is *broken* (or reduced), because the direction  $\hat{B}$  of the magnetic field is now uniquely defined by its presence. Because the spectral lines of the atomic emissions are split into multiple, nearby wavelengths by the application of a magnetic field (as demonstrated by Zeeman), the atoms are influenced by the field and are thus aware that *the direction  $\hat{B}$  is no longer equivalent to other spatial directions in the gas*. This is what is meant by the phrase *broken symmetry*: the originally isotropic spatial structure of the gas is now made less symmetric by the field's presence. However, the symmetry of the spatial structure is reduced in almost the gentlest way possible: the interior of the gas is still homogeneous (on average), and only one direction (or Cartesian coordinate axis) has been defined by the direction of the uniform magnetic field; the gas remains rotationally symmetric about the applied field direction.

We now ask the following question: of all the possible simple-harmonic, periodic orbits available for an oscillating atomic charge, what orbital shapes are consistent with this reduced symmetry, that is, what orbital shapes (in 3-D space) require reference to only one spatial direction (or axis)? As shown in Figure 3, the only available orbital shapes are: (1) a linear oscillation along the specified axis, and (2) circular motion in a plane perpendicular to the axis. Consider these fundamental orbits shown in Figure 3. Because the applied magnetic field is described by a vector, the axis it defines is asymmetrical in the sense that the direction parallel to  $\hat{B}$  is distinguishable from the direction antiparallel to  $\hat{B}$ . Consequently, right-handed and left-handed circular orbits are also distinguishable, giving the three distinct simple-harmonic orbits shown.

Incidentally, in the limit of a vanishingly-small magnetic field, all three of the simple-harmonic orbits shown in Figure 3 would have the same angular frequency of motion,  $\omega_0$ , because of the spherical symmetry of the potential in which the charge moves. These three orbits are not only linearly independent (none can be formed from a linear combination of the others), but also orthogonal, and they form a basis from which all other simple-harmonic orbits with frequency  $\omega_0$  may be constructed through linear combinations of them (by choosing the appropriate amplitude and phase of each of the three basis orbits). If there were no magnetic field present,

**Figure 3: Orbital shapes which honor the reduced directional symmetries of the hot gas once a magnetic field is applied. The description of each orbit must require the specification of only one unique axis, which is that axis defined by the field direction. Thus only two orbit shapes are permitted: oscillation along the axis and circular motion in a plane normal to the axis. The circular motion may be right-handed or left-handed, giving the three distinct simple-harmonic orbits shown.**



then one would also be free to choose the direction of the axis defining these basis orbits, again because of the overall average spherical symmetry of the hot gas.

In the presence of a nonzero magnetic field, however, prudence would dictate that these basis orbits be aligned with the field as in Figure 3. Because each of these three orbits has a relationship to the magnetic field vector which differs from the other two (remember, even the right-handed and left-handed circular orbits can be expected to react differently to the field's presence), one might expect that each could have its angular frequency affected by the magnetic field independently of how the field affects the others. As we shall see in the next section, these are indeed the classical orbits whose individual frequency shifts result in spectral line splitting as described by Lorentz's theory of the Zeeman Effect.

### ***Harmonic oscillator with an applied magnetic field***

We now shift our focus from symmetry considerations to analyze the forces generated on our charge by an applied magnetic field as it oscillates in its harmonic oscillator potential, again using classical physics for the calculations. Taking the center of the potential well as the origin of our Cartesian coordinate system, the 3-dimensional, Hook's law force on the charge at position  $\vec{r} = x\hat{x} + y\hat{y} + z\hat{z}$  was originally (before the application of  $\vec{B}$ )

$$\begin{aligned}\vec{F} &= -m\omega_0^2\vec{r} = m\ddot{\vec{r}} \\ \therefore \ddot{x} &= -\omega_0^2 x; \quad \ddot{y} = -\omega_0^2 y; \quad \ddot{z} = -\omega_0^2 z\end{aligned}\tag{27.5}$$

where  $\omega_0$  is the charge's angular frequency of oscillation about the center of the potential well. Applying a magnetic field oriented along our system's  $z$ -axis,  $\vec{B} = B\hat{z}$ , the field will exert a Lorentz force on the moving charge:

$$\begin{aligned}\vec{F}_B &= q\dot{\vec{r}} \times \vec{B} = qB(\dot{x}\hat{x} + \dot{y}\hat{y} + \dot{z}\hat{z}) \times \hat{z} = qB(\dot{y}\hat{x} - \dot{x}\hat{y}) = m\ddot{\vec{r}}_B \\ \therefore \ddot{x}_B &= \frac{q}{m}B\dot{y}; \quad \ddot{y}_B = -\frac{q}{m}B\dot{x}; \quad \ddot{z}_B = 0\end{aligned}\tag{27.6}$$

The  $B$  subscripts in (27.6) remind us that these are the additional accelerations introduced by the magnetic field. Combining this result with that of (27.5) results in the differential equations for the charge's position coordinates when subject to both the original harmonic oscillator potential as well as the magnetic field:

$$\ddot{x} = \frac{q}{m}B\dot{y} - \omega_0^2 x; \quad \ddot{y} = -\frac{q}{m}B\dot{x} - \omega_0^2 y; \quad \ddot{z} = -\omega_0^2 z\tag{27.7}$$

The differential equation for the  $z$  coordinate is unchanged by the presence of the field, and its solution is just a sinusoidal oscillation along the  $z$ -axis. On the other hand, the field has coupled the two 2<sup>nd</sup>-order differential equations for the  $x$  and  $y$  coordinates. As shown in Prelab Problem



2 on page 20, the two solutions to the coupled equations for  $x$  and  $y$  correspond to circular motions in the  $x$ - $y$  plane, orbiting in opposite senses, with the two angular frequencies

$$\omega_+ = \omega_0 - \frac{q}{2m}B; \quad \omega_- = -\left(\omega_0 + \frac{q}{2m}B\right) \quad (27.8)$$

(assuming that  $\omega_0 \gg |q/2m|B$ ). These three solutions to (27.7), a linear oscillation along  $\hat{B}$  with angular frequency  $\omega_0$  and two circular orbits around  $\hat{B}$  at frequencies slightly above and below  $\omega_0$ , are the elements of the set of *normal modes* for the classical motion of our charge in the presence of a uniform magnetic field. Note that these are the same orbital motions we identified using purely symmetry considerations and depicted in Figure 3 on page 5. If a charge were originally in some linear combination of these three modes before the application of the field, then as the field is turned on, the frequencies of the modes would shift, and the charge would now have a complicated, no longer generally elliptical, motion composed of the separate oscillations shown in Figure 3, emitting three components of radiation each with its own frequency and polarization relative to an observer.

### ***Consequences of the analysis for experimental measurements***

The satisfying consistency between the symmetry considerations and the dynamical calculations outlined above provides some level of confidence that this approach to the analysis of Zeeman splitting may prove useful to the understanding of the internal workings of atoms. If this classical analysis of charge motion during spectral line generation applies to atomic systems, then we expect that the application of a magnetic field to an atom should ***split each observed spectral line into three lines***:

- A line remaining at the original spectral line frequency  $\omega_0$  and with linear polarization parallel to the direction of the magnetic field, generated by oscillating charge motion along  $\hat{B}$  (the  $z$ -axis in the analysis of equations (27.7)).
- Two lines whose frequencies change by  $\Delta\omega = \pm(q/2m)B$  away from the original line frequency  $\omega_0$ . Generated by circular charge motions in a plane normal to  $\hat{B}$ , their polarizations will vary from linear when observed from a direction perpendicular to  $\hat{B}$  to circular when observed from a direction parallel to  $\hat{B}$ .

Importantly, the frequency shifts of the two “daughter” spectral lines should be proportional to the magnetic field strength  $B$  and the charge’s charge-to-mass ratio  $q/m$ . As shown in Prelab Problem 2 on page 20, the senses of the circular (or elliptical) polarizations of the two shifted lines (when observed from an appropriate direction) will depend on the sign of the charge  $q$ .

**As mentioned in the Introduction, Zeeman and Lorentz applied this theory to observations of spectral line splitting and determined that spectral lines could be generated by motions of J. J. Thompson's electron within an atom (they got the same sign and magnitude for  $q/m$ ), thus for the first time clearly identifying an atomic constituent and providing some evidence of the internal workings of an atom.**

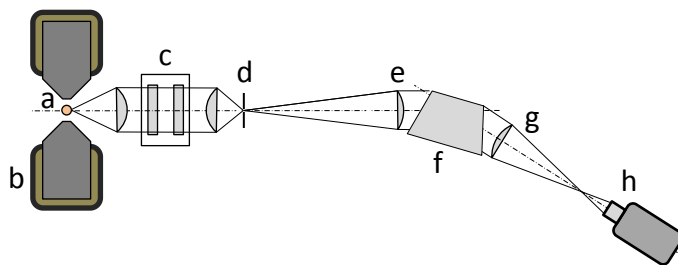
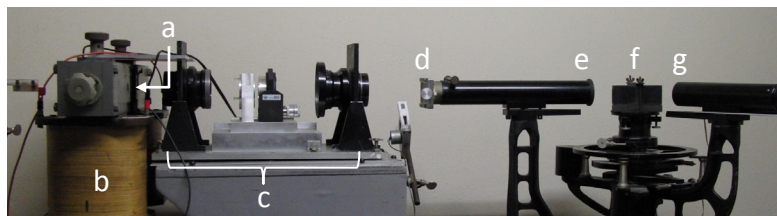
One last, very important point about the application of this simple, classical theory: if it should prove inadequate to describe the observed spectral line splitting by an applied magnetic field, *then there must be additional physics going on within an atom* which the classical theory is unable to elucidate. Of course, and as you will most definitely find as you conduct the experiment, this classical theory is indeed unable to adequately describe the behavior of electrons in atoms—the *quantum theory* is absolutely necessary to make sense of how the electrons behave. On the other hand, a very few spectral lines do exhibit splitting which is well-described by the Zeeman-Lorentz theory, especially in lighter atoms such as neon, and thus the identification of the electron as an atomic constituent using the theory was still a reasonable conclusion, even though it is not the whole story.

## THE APPARATUS

A lamp containing neon gas is inserted between the pole pieces of a large electromagnet. The light from the lamp is collimated and passed through a *Fabry-Pérot interferometer* (described below) before being focused onto the input slit of a *prism spectrometer*. The spectrometer output is detected by a sensitive video camera; its image of the spectral lines is displayed on a video monitor. The optical arrangement is shown in Figure 4. The large electromagnet and its associated power supply can generate fields of up to just under 2 Tesla.

**Figure 4: Side-view photo and top-view diagram of the optical arrangement of the experiment apparatus.**

(a) neon lamp; (b) electromagnet; (c) Fabry-Pérot interferometer with collimation lenses; (d) spectrometer entrance slit; (e), (g) prism spectrometer lenses; (f) prism; (h) low-light video camera (not shown in the photo).



The prism spectrometer (components d–h in Figure 4) forms an image of its entrance slit on the video camera's image plane. Because the prism's index of refraction depends on wavelength (higher index at shorter wavelengths), the prism will bend light of different colors through different angles. Thus the spectrometer forms multiple images of the slit at its output, one for each line wavelength in the neon lamp's spectrum, forming an image similar to the spectrum shown in Figure 1. Because the camera and its monitor are monochrome the image on the monitor is in shades of gray. Additionally, the camera is mounted on its side, so the spectral lines on the monitor are horizontal rather than the vertical lines of Figure 1.

### *Fabry-Pérot interferometer*

The prism spectrometer's wavelength resolution is woefully inadequate to detect the spectral line splitting due to the Zeeman Effect (see Prelab Problem 4 on page 21). To resolve the very small wavelength shifts involved (less than an Ångstrom), the apparatus uses a small *Fabry-Pérot interferometer* (or *etalon*).<sup>7</sup> The etalon uses a pair of partially-reflective mirrors to form a resonant cavity. A plane wave from the source is incident on one mirror, and some of its light

<sup>7</sup> The French physicists Charles Fabry and Alfred Pérot first described their interferometer in an 1897 paper (Mulligan, 1997). Their invention remains of great importance today; for example, it is a key element of the design of the LIGO interferometer.

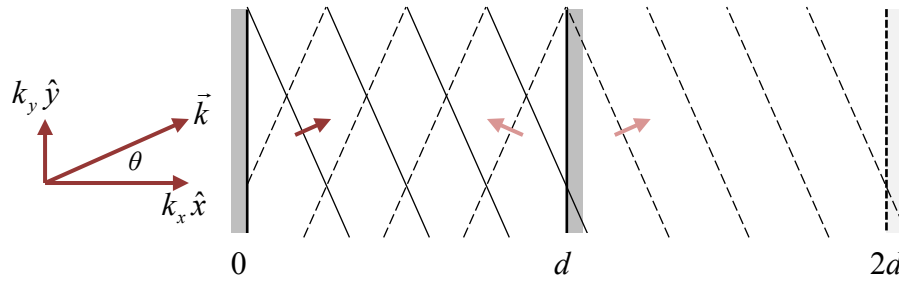


**Figure 5: A plane wave with wave vector  $\vec{k}$  leaves the left-hand mirror (at position  $x = 0$ ) and reflects off the mirror at  $x = d$ . Wave crests (lines of constant phase) in the original wave are shown by the thin solid lines; the reflected wave's crests are denoted by the thin dashed lines. The phase of the reflected wave as it returns to the left-hand mirror is the same as that of the original wave if it were to continue on to a surface at position  $x = 2d$  (dashed wave crests continuing on to the right past the mirror at  $d$ ).**

enters the cavity. Energy filling the cavity can gradually escape via the other partially-reflective mirror and continue on to the prism spectrometer. At a resonance of the cavity, the light contained within it can become greatly intensified, and therefore so can the power which escapes through the mirrors. The cavity acts as a highly selective (high-Q) filter, or, for this application, an analog of a very high resolution diffraction grating.

To understand how the etalon works, first consider the case of two ideal, parallel mirrors with a plane wave reflecting back and forth between them at some angle  $\theta$  (Figure 5). The left-hand mirror in the figure fills the  $y$ - $z$  plane at  $x = 0$ . The right-hand mirror fills a parallel plane at position  $x = d$ . The plane wave leaving the left-hand mirror has wave vector  $\vec{k} = k_x \hat{x} + k_y \hat{y}$ , as illustrated in the figure. *Physics 6 General Appendix D: The Wave Vector* shows that the phase of this wave at any point in space is then given by  $\phi(\vec{r}) = \vec{k} \cdot \vec{r} = k_x x + k_y y$ . The wave reflects from the right-hand mirror and arrives back at the left-hand mirror. At a resonance of this optical cavity, the two waves interfere constructively, which means that they are in phase at every point on either mirror; in particular, they must be in phase at all points on the left-hand mirror.<sup>8</sup>

The reflected wave's phase upon arrival at the left-hand mirror is the same as what the original wave's phase would have been if it had continued on past the mirror at  $d$  and arrived at a plane at  $x = 2d$ , as illustrated in Figure 5. The original wave's phase in the plane  $x = 0$  is  $\phi(0, y, z) = k_y y$ . Its phase in the plane  $x = 2d$  is  $\phi(2d, y, z) = k_x 2d + k_y y$ , which is the same as the reflected wave's phase as it returns to the left-hand mirror. For the waves to be in phase at the left-hand mirror, their difference must be a multiple of  $2\pi$ , so:

$$\begin{aligned} \phi(2d, y, z) - \phi(0, y, z) &= 2dk_x = 2\pi m \quad (\text{integer } m) \\ \therefore k_x &= m(\pi/d) \end{aligned} \tag{27.9}$$

<sup>8</sup> We assume for this discussion that the amplitude reflection coefficient of each mirror  $\Gamma = 1$ . Similar results would obtain for other choices for the relative phase of each mirror's reflection, but the algebra for the more general case is messier and not particularly "illuminating."

Equation (27.9) with  $m$  a positive integer is the same criterion found for a 1-D resonant cavity with partially-reflective terminations analyzed in *Physics 6 General Appendix A: Transmission Line Resonance due to Reflections* (see the text surrounding equation (32) in that document).

Since  $k_x = k \cos \theta$ , where  $k = 2\pi/\lambda$  is the magnitude of the wave vector  $\vec{k}$ , we can rephrase the resonance requirement (27.9) as:

$$\cos \theta = m \frac{\lambda}{2d}; \quad \text{at resonance } m \in \mathbb{N} \quad (27.10)$$

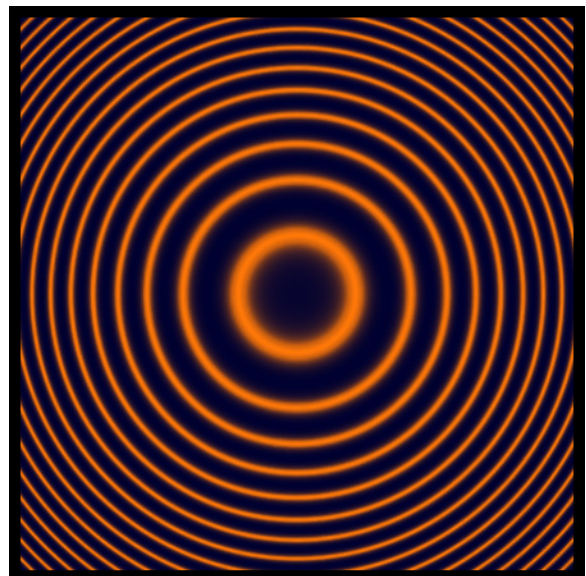
The positive number  $m$  is called the *order* corresponding to an angle  $\theta$  of the plane wave's wave vector, and it assumes an integer value at each resonance. The order  $m$  is obviously greatest for  $\theta = 0$  (where  $m = 2d/\lambda$ ) and decreases toward 0 as  $\theta \rightarrow \pi/2$ .

For light of a given wavelength  $\lambda$  and a much larger separation of the mirrors  $d \gg \lambda$ , the etalon will display many resonances in the region near  $\theta = 0$ . In the 3-dimensional cavity, the set of all wave vectors of waves with wavelength  $\lambda$  and making an angle  $\theta$  with the  $x$ -axis will form a cone about that axis (the  $x$ -axis is perpendicular to the planes of the two etalon mirrors). If *monochromatic* light (all at the same wavelength) is present in the cavity as various plane waves in every direction, the resonances will form bright circles (*interference fringes*), one for each integer value of the order  $m$  (Figure 6). In the space between a pair of the bright fringes shown in Figure 6, the angle  $\theta$  corresponds to a value of the order  $m$  which is not an integer.

Assume that a plane wave propagates in the cavity at a fixed, small angle  $\theta$ . If its wavelength  $\lambda$  changes by a very small amount  $\Delta\lambda \ll \lambda$ , then the change in the order  $m$  corresponding to a fixed  $\theta$  (using equation (27.10)) is, to first order in  $\Delta\lambda/\lambda$ , approximately

$$\Delta m \approx \Delta\lambda \times \left. \frac{dm}{d\lambda} \right|_{\theta \text{ constant}} = -m \frac{\Delta\lambda}{\lambda} = -\frac{2d}{\lambda} \frac{\Delta\lambda}{\lambda} \cos \theta$$

**Figure 6: Simulated fringe pattern at the output of a Fabry-Pérot interferometer (etalon) when exposed to light of a single wavelength. Each bright ring represents a resonance of the cavity corresponding to a particular order  $m$  and corresponding angle  $\theta$ . The mirror separation was chosen to be 13.2mm and the orange light wavelength  $\lambda$  was 595.0nm. The range of  $\theta$  shown is up to 0.02 radians about the central axis (a bit more than  $1^\circ$ ). The innermost bright ring corresponds to order  $m = 44,403$ ; its  $\theta = 0.23^\circ$  (equation (27.10)). The reflectivity of the mirrors was assumed to be approximately 50%, which determined the widths of the rings and, consequently, the ultimate resolution of the system.**



**Constant  $\theta$ , change in  $m$  due to  $\Delta\lambda$ :** 
$$\Delta m \approx -\frac{2d}{\lambda} \times \frac{\Delta\lambda}{\lambda} \quad (27.11)$$

We've approximated  $\cos\theta \approx 1$  in (27.11). This important expression shows that, because  $d \gg \lambda$ , the change in order  $\Delta m$  will be much larger than the fractional change in wavelength  $\Delta\lambda/\lambda$ . It is this property of the Fabry-Pérot interferometer which we will exploit to resolve the very small wavelength shifts introduced by the Zeeman Effect.

On the other hand, equation (27.10) explicitly indicates how the angle  $\theta$  would change in response to a small wavelength change if we hold the order  $m$  constant. For example, the locations of the bright fringes in Figure 6 will change their radii slightly if the wavelength undergoes a small shift  $\Delta\lambda \ll \lambda$ . We want to determine how to express this shift in angle  $\Delta\theta$  of a particular bright fringe (at which the order  $m$  equals some integer) as a corresponding shift in order  $\Delta m$  of light at the original wavelength. For example if the resulting  $\Delta m = 0.5$ , then the bright fringe will have shifted to a new position approximately mid-way between the original positions of the fringes corresponding to orders  $m$  and  $m+1$ . Using (27.10):

$$\Delta\theta \text{ due to } \Delta\lambda, \text{ with } m \text{ constant: } \cos(\theta + \Delta\theta) = m \frac{\lambda + \Delta\lambda}{2d} = m \frac{\lambda}{2d} + m \frac{\Delta\lambda}{2d}$$

$$\Delta\theta \text{ due to } \Delta m, \text{ with } \lambda \text{ constant: } \cos(\theta + \Delta\theta) = (m + \Delta m) \frac{\lambda}{2d} = m \frac{\lambda}{2d} + \Delta m \frac{\lambda}{2d}$$

$$\text{equating the two expressions: } \therefore \Delta m \lambda = m \Delta\lambda = \Delta\lambda \frac{2d}{\lambda} \cos\theta \approx \Delta\lambda \frac{2d}{\lambda}$$

**Constant  $m$  (feature), new  $\theta$  referred to original  $m(\lambda)$ :** 
$$\Delta m \approx \frac{2d}{\lambda} \times \frac{\Delta\lambda}{\lambda} \quad (27.12)$$

Again, we've approximated  $\cos\theta \approx 1$ . Note that this expression is just the negative of that in (27.11). To understand what is meant by (27.12), consider the example illustrated in Figure 7 on page 13. The middle pattern in the figure is a slice through part of the fringe pattern shown in Figure 6, showing the center of the pattern (behind the text identifying the wavelength, " $\lambda_0 = 595.0 \text{ nm}$ "), as well as a few of the innermost fringes to its right. The order numbers of these fringes,  $m = 44,403$  to  $m = 44,397$ , are also identified. The images above and below the middle one show the fringe patterns produced by very slightly shifting the wavelength: as indicated in the figure,  $\Delta\lambda = \pm 4.7 \times 10^{-3} \text{ nm}$ , giving  $\Delta\lambda/\lambda$  of less than 8 parts per million. With  $d = 13.2 \text{ mm}$ , the fringe shifts are quite apparent, and equation (27.12) gives  $\Delta m = \pm 1/3$ .

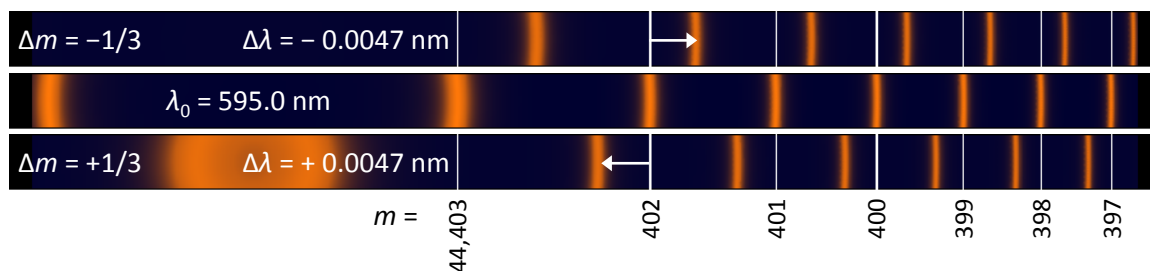


*Figure 7: An example to illustrate the meaning of the expression (27.12). The images show a slice of a part of the pattern in Figure 6 containing a few of the central-most bright fringes. The upper and lower fringe patterns result from shifting the original wavelength by the tiny amounts shown. The order numbers of these new, shifted fringes still equal the corresponding  $m$  values in the original pattern, but their new positions, when referred to the original fringe positions, have shifted by an angle equivalent to an order change of  $\Delta m = \pm 1/3$ .*

**The interpretation of this resulting change in the order  $\Delta m$  is as an indication of the magnitude and direction of the fringe shift relative to the gap between adjacent fringes (since the fringes appear at integer values for  $m$ ,  $\Delta m = 1$  for the width of each gap).**

In this case the fringes have each moved from their original positions by about  $1/3$  of the fringe spacing (arrows in the shifted fringe images for the case of the  $m = 44,402$  fringe). Note that in the lower image in *Figure 7*, the wavelength shift has moved the innermost bright fringe ( $m = 44,403$ ) close to the etalon axis, forming a bright, disk-shaped central fringe. On the other hand, the interpretation of equation (27.11) is that its  $\Delta m$  gives the position formerly occupied by the original fringe relative to its new, shifted position, thus the change in sign relative to (27.12).

Some final comments about the accuracies of keeping terms only to first order in  $\Delta\lambda/\lambda$  and of approximating  $\cos\theta \approx 1$  in equations (27.11) and (27.12). As noted above for the example shown in *Figure 7*,  $\Delta\lambda/\lambda < 10^{-5}$  for  $\Delta m = 1/3$ . Even for  $\Delta m = 2$  the resulting  $\Delta\lambda/\lambda < 5 \times 10^{-5}$ , so keeping only terms to first order in  $\Delta\lambda/\lambda$  results in an error of only about 0.01%. As for  $\cos\theta$ , the maximum  $\theta$  shown in *Figure 7* is  $1^\circ$ , so  $1 - \cos(1^\circ) \approx 1.5 \times 10^{-4}$ , and at the position of the fringe with  $m = 44,401$  shown in the middle image of *Figure 7*,  $1 - \cos\theta \approx 5.3 \times 10^{-5}$ , again resulting in an error of less than 0.01%.

### *Viewing Zeeman splitting*

The neon lamp emits many spectral lines (a few of the brighter ones are shown in Figure 1 on page 1), and they all exhibit splitting in response to an applied magnetic field. All of these various wavelengths are filtered by the etalon and then focused on the entrance slit to the prism spectrometer (Figure 4). The prism separates the spectral lines, so that in the video camera's monitor, each spectral line is isolated and displays etalon fringes similar to those in *Figure 7*. The camera and monitor are monochrome, however, so all spectral lines are displayed as gray.

Figure 8 below shows a simulated example of the camera's image of a single spectral line, the red 626.6nm normal Zeeman line you will primarily use for data taking. With no applied  $B$ , the fringe pattern is that for the single, unperturbed line wavelength. As the magnetic field is increased, two "satellite" fringes separate from each original fringe. The magnitude of the change in etalon order  $\Delta m$  for each of these satellite fringes increases linearly with  $B$ , as derived in the solution to Prelab Problem 5 on page 21.

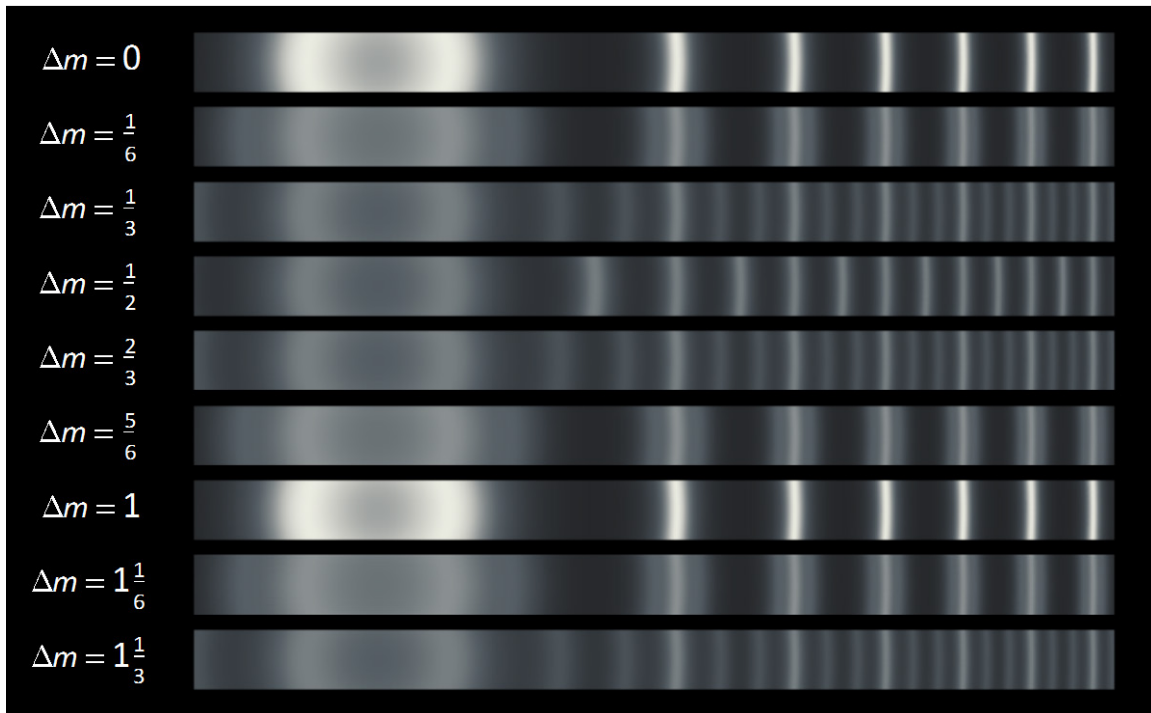


Figure 8: Simulated Zeeman splitting of the neon 626.6nm spectral line, as seen through the experiment's apparatus using the Fabry-Pérot etalon and the prism spectrometer. As in the images shown in Figure 7, the center of the etalon fringe pattern is about 1/5 of the way over from the left edge of each image. The mirror separation  $d = 13.2\text{mm}$ , and the step in  $\Delta\lambda$  between successive images is about  $2.48 \times 10^{-3}\text{nm}$ . Each "satellite" fringe (a fringe whose wavelength varies with  $B$ -field) has a lower intensity than its associated stationary fringe.

Note that whenever  $|\Delta m| = 1/3, 2/3, 4/3, \text{etc.}$ , then the satellite fringes are spaced symmetrically within the gaps between the stationary fringes; when  $|\Delta m| = 1/2, 3/2, \text{etc.}$ , then two satellites merge to form a single fringe between the stationary ones; and when  $|\Delta m| = 1, 2, \text{etc.}$ , then all fringes recombine to reproduce the original, 0-field fringe pattern.



### *Hall probe*

A Hall probe is used to accurately measure the magnetic field to which the neon lamp is exposed. The Hall probe sensor is a small, thin, rectangular semiconductor wafer. Current  $I_H$  from a power supply flows across the wafer from one edge to the opposite, and the voltage  $V_H$  across the other two edges is measured by a sensitive voltmeter. Ideally, the measured  $V_H$  is proportional to the product of the component of the magnetic field normal to the surface of the wafer,  $B_{\perp}$ , and the current  $I_H$ , because a Lorentz force generated by the field causes the charge carriers in the wafer to be deflected toward one edge as they travel through it. This build-up of mobile charge carrier density along one edge in the (overall neutral) piece of material creates an electric field orthogonal to the direction of current flow, which is sensed by  $V_H$ .

You calibrate the hall probe in two steps:

- (1) Hold the probe far from any magnets and oriented parallel to the Earth's field. In this case  $V_H = 0$ . Use the offset or null function of the voltmeter attached to the probe to zero out any residual voltage reading.
- (2) Insert the probe into the calibration magnet (a small, permanent magnet) and adjust the Hall probe power supply current until the measured  $V_H$  corresponds to the value of the calibration magnet field  $B$ .

Following calibration the Hall probe is inserted into a bracket to the left of the electromagnet. Once the neon lamp is lowered out of the gap between the magnet pole pieces, the Hall probe bracket may be slid forward to insert the probe sensor into the gap, measuring the applied field (Figure 9).

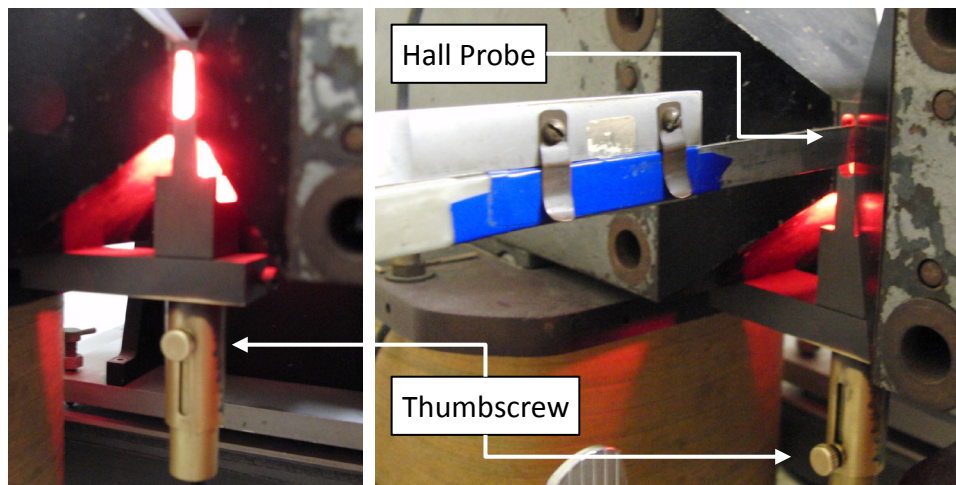


**Figure 9:** The back side of the magnet and neon lamp support showing where the Hall probe sensor is inserted for a magnetic field measurement. The thumbscrew is very slightly loosened so that the lamp may be lowered out of the gap between the magnet pole pieces. The hall probe is then guided into the gap by sliding its support bracket forward.

## PROCEDURE

The procedure divides naturally into four parts:

- Calibration and alignment of the etalon and Hall probe
- Spectrometer adjustments and identification of the normal Zeeman spectral lines
- Data gathering for various magnetic field strength settings
- Investigation of line polarizations

Each of these parts will be discussed below.

### *Calibration and Alignment*

#### *Hall probe*

**When raising or lowering the neon lamp, MAKE SURE YOU SUPPORT THE LAMP FROM BELOW so that if you inadvertently remove its thumbscrew, the lamp does not fall out of the magnet gap and break.**

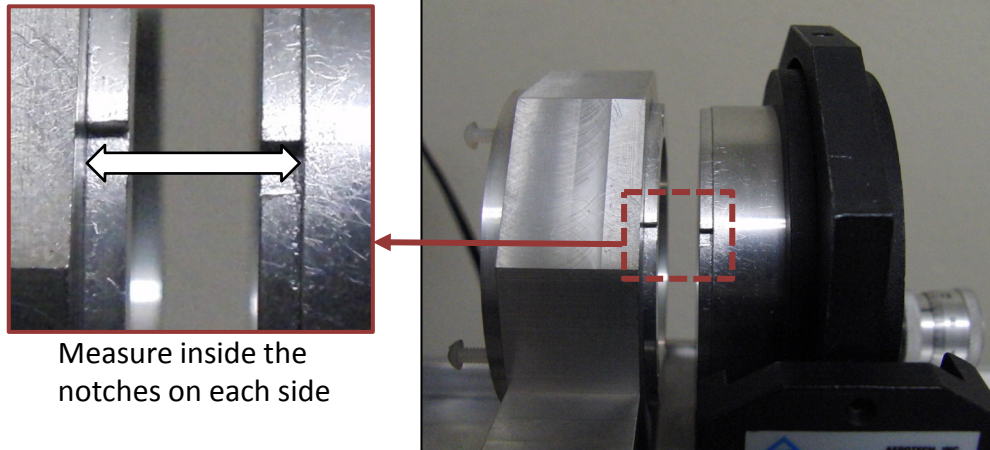
**If the lamp should become stuck with the thumbscrew removed, DO NOT reduce the magnetic field while leaving the lamp unattended, because it may then fall and break.**

Calibrate the Hall probe as described in the *Hall probe* section (page 15) and mount it in its support bracket. With the neon lamp lowered out of the magnet pole-piece gap (see Figure 9), adjust the hall probe support bracket so that it slides the probe smoothly into the center of the pole-piece gap. Make sure that the probe wiring is not caught on anything that could break the wires, and make sure that the wiring is positioned so that you will not inadvertently snag or pull and break one of the wires while performing a magnetic field measurement.

#### *Fabry-Pérot etalon*

Measure the separation distance  $d$  of the two etalon mirrors by first carefully lifting the etalon mirror assembly by its base plate and removing it from the apparatus to a table, then measuring  $d$  using calipers. Each mirror retaining ring has a pair of notches cut into it as shown in Figure 10 on page 17. The distance between the two mirrors may be measured by inserting calipers into the notches as shown in the figure; a pair of notches is available on each side of the mirror assembly. Once the measurements are complete, carefully reposition the etalon assembly in the apparatus.

Following measurement, the etalon mirrors must be adjusted so that they are parallel to within a small fraction of a wavelength of light. Unless this adjustment is done properly, the interference fringes produced by the etalon will have poor contrast and the instrument will fail to resolve the Zeeman splitting of the neon spectral lines. You perform the adjustment while looking through the etalon at the neon lamp and observing the interference fringes. Remove the large collimating lens located between the etalon assembly and the spectrometer entrance slit. Once the lens is removed you will have enough space to look through the etalon assembly at the neon lamp.



Measure inside the notches on each side

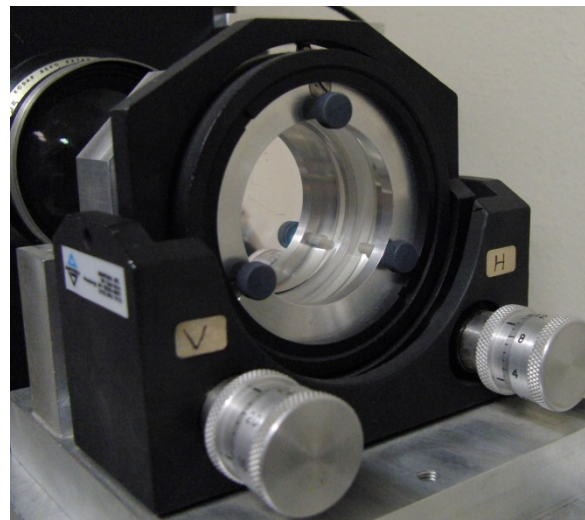
**Figure 10:** The etalon mirrors are pressed against the two retaining rings on the inside surfaces of the mirror mounts. Measure the mirror separation by inserting calipers into the notches in the retaining rings (there is a pair on each side of the mounts; only one pair is visible in the photos).

The interference fringes will appear as dark, concentric arcs across the image of the lamp, centered on a dark disk or ring somewhere in the lower half of the image of the lamp. As you move your head to look through different parts of the etalon mirror, the central fringe disk will change size and color as the surrounding arcs move toward or away from it. The fringes move radially inward or outward as you move your head because the distance  $d$  between the mirrors varies: the mirrors are not parallel.

Make **VERY SLIGHT** adjustments to the mirror gimbal micrometer screws to make the mirrors parallel (Figure 11). When the mirrors are parallel, the central interference disk will not change size or color and the fringe arcs will not move radially inward or outward as you move your head to look through different parts of the etalon mirror. **If you notice any changes to the fringe pattern, then you must continue to work to improve the alignment.** Once the alignment is complete, carefully replace the collimating lens.

**Figure 11:** The etalon mirror mount showing the gimbal adjustment micrometers. Each is labelled: “V” for vertical alignment, “H” for horizontal. Only the knobs with the numerical scales should be adjusted (the scales are in microns). After each small adjustment of one of the micrometers, recheck the alignment by moving your head while watching the interference fringes.

**Do not touch the etalon adjustment knobs or the mirror mounts while checking the alignment.**



### ***Spectrometer adjustments and line identification***

Rotate the spectrometer imaging telescope (the one with the camera) toward you by pulling on its support brace; you should eventually see spectral lines appear in the camera's video monitor. Adjust the slit width so that the spectral lines are broad enough to clearly see the bright interference fringes. Adjust the camera focus and f-stop to optimize the brightness and sharpness of the interference fringes on the video monitor.

The two normal Zeeman spectral lines of neon are at 585.2nm (yellow) and 626.6nm (red). The 585.2nm line is the shortest wavelength bright yellow line in the neon spectrum. Use this fact to identify this line on the video monitor screen and rotate the imaging telescope to place it near the top of the video screen. The 626.6nm line will then also be on the monitor screen, but you must identify it.

**Do not turn the magnet power supply on or off unless its output voltage is turned down all the way to 0. Otherwise, the large voltage induced by the magnet inductance to the sudden change of current can destroy the power supply.**

Activate the magnet power supply and increase the current through the electromagnet. You should see Zeeman splitting of all of the spectral line fringes displayed on the monitor. If the fringes become generally very hard to see, check the camera focus. If they remain very faint or blurry, then the etalon is probably not properly adjusted. The 585.2nm line normally has fringes which are very hard to see, but you can readily identify Zeeman splittings with  $\Delta m = 1$  or  $\Delta m = 2$ , because for these order shifts the original, 0-field fringe pattern reappears (look again at Figure 8 on page 14). From the answer to Prelab Problem 5 you know that both normal Zeeman lines have the same  $\Delta m$  fringe shift at all field settings, so identify the 626.6nm line by finding the only other line in the spectrum with fringe splittings matching the 585.2nm line at both  $\Delta m = 1$  and  $\Delta m = 2$ .

**The 626.6nm normal Zeeman spectral line should have satellite fringes which are visible at intermediate (non-integer)  $\Delta m$  values. If they are not, then the etalon probably needs adjustment.**

### ***Data acquisition***

Once you have identified the 626.6nm normal Zeeman line, use this line for data taking. Adjust the magnetic field to establish various identifiable  $\Delta m$  settings from  $\Delta m = 1/3$  to  $\Delta m = 2$  ( $\Delta m = 1/3, 1/2, 2/3, 1, 4/3$ , etc). For each setting, carefully lower the neon lamp and measure the magnetic field using the Hall probe. You will run through the range of  $\Delta m$  settings several times, repeating the measurements.

### *Investigation of line polarizations*

A rotatable linear polarizer is available which may be positioned in front of the spectrometer entrance slit; your TA can show you how to use it. By rotating the polarizer you can check Lorentz's theory regarding the fringe polarizations.

### *Securing the apparatus*

- Adjust the magnet power supply to 0 and then turn it off.
- Turn off the neon lamp.
- Carefully remove the Hall probe from its support bracket and insert it into the calibration magnet.
- Rotate the spectrometer imaging telescope so that the camera is no longer an obstacle to people walking past the apparatus.

**Make sure that you have accurately measured the etalon mirror separation before leaving the lab!**

### **ANALYSIS**

Create a text file with a single  $(\Delta m, B)$  data value pair on each line (as in the *CurveFit* sample data file *Zeeman.dat*), so that you have several lines for each  $\Delta m$ , each line with its own  $\Delta m$  and a single measured  $B$  value (separate the values by a space or tab). Load this file into *CurveFit*, and you may use the *CurveFit* palette menu selection *Modify data points: Basic data manipulations: Analyze Y data and assign  $\sigma$ 's* to calculate the uncertainties in your  $B$  measurements for each  $\Delta m$  value.

Fit the  $\Delta m$  vs.  $B$  data to test Lorentz's theoretical prediction for the normal Zeeman spectral line you used. Should the fit be linear (see Prelab Problem 5)? Why should you fit using a linear relation  $y = a + bx$  rather than the strict proportion  $y = bx$ ? Should the intercept be consistent with 0? What calibration issue in your experiment might cause a nonzero intercept? Determine a value and uncertainty for  $e/m$  of the electron from your fit. What are the major sources of systematic error? How does your value compare to the currently accepted experimental estimate for  $e/m$ ?

## PRELAB PROBLEMS

1. Consider the orbital motions depicted in Figure 3 on page 5 of the text. For a distant observer located in the plane containing the circular orbits, and for each of the three orbital paths shown, what would be the resulting polarization at the observer's location of the electromagnetic radiation emitted by a moving charge if it were to follow that path? What if the distant observer were instead located somewhere on the axis defined by the magnetic field direction? Which is the situation applicable to the experimental set-up you will use?
2. Consider the pair of coupled, 2<sup>nd</sup>-order differential equations for  $x$  and  $y$  in (27.7), repeated below:

$$\begin{aligned}\ddot{x} &= +\frac{q}{m}B\dot{y} - \omega_0^2 x \\ \ddot{y} &= -\frac{q}{m}B\dot{x} - \omega_0^2 y\end{aligned}$$

- a) Show that the functions  $x(t) = \cos \omega t$ ,  $y(t) = \sin \omega t$  solve these differential equations, for a suitable choice for the angular frequency  $\omega$ . Show that the two allowed values of  $\omega$  are given by:

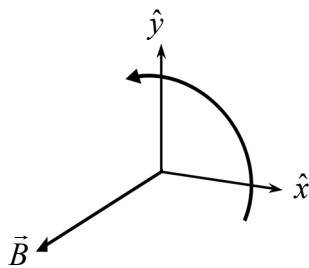
$$\omega = -\frac{1}{2}\omega_B \pm \sqrt{\omega_0^2 + \left(\frac{1}{2}\omega_B\right)^2}$$

where the *cyclotron frequency*  $\omega_B \equiv (q/m)B$ .

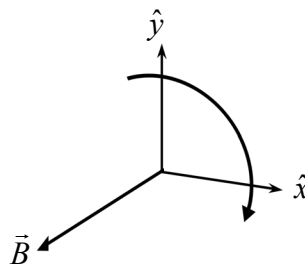
- b) Taking  $\omega_0$  to be positive, then if  $|\omega_B| \ll \omega_0$ , the two values for  $\omega$  simplify to:

$$\omega = \omega_0 - \frac{1}{2}\omega_B; \quad \omega = -\left(\omega_0 + \frac{1}{2}\omega_B\right)$$

Each solution represents circular motion around the origin in the  $x$ - $y$  plane. What is the sign of  $\omega$  for the solution corresponding to each sense of rotation about the  $z$ -axis shown below (remember that  $\vec{B}$  is in the same direction as  $\hat{z}$ )?



Right-hand sense around  $\vec{B}$  ( $\hat{z}$ ).



Left-hand sense around  $\vec{B}$  ( $\hat{z}$ ).

- c) For which sense of rotation shown above will  $|\omega| > \omega_0$  if the moving charge is an electron ( $q < 0$ )?

3. Calculate an estimate of the value for the cyclotron frequency  $|\omega_B| = |q/m|B$  for an electron in a 1 Tesla magnetic field, using the following method (which will be good practice for many calculations in Physics 7):
- Since  $B$  is given in SI units, using SI units throughout will result in the SI value for  $\omega$ , which is, naturally, rad/sec.
  - The magnitude of the electron charge,  $e$ , is also used as a unit of charge, so let's stick with that, rather than looking up its SI value (in coulombs). Thus we need a value for  $m$  which is compatible. Therefore we use the *rest energy* of the electron in *electron volts* (eV),  $m \rightarrow mc^2 = 0.511 \times 10^6$  eV. This means that  $e/(mc^2)$  has units of  $\text{volt}^{-1}$ , an SI unit (since the “e” in eV in the denominator cancels the numerator’s electron charge  $e$ ).
  - Therefore  $|q/m| = c^2/(mc^2/e)$ , and we need only know the speed of light  $c$  in SI units and the electron’s rest energy in eV to determine the electron charge/mass ratio in SI units ( $\text{coul/kg} = \text{meter}^2\text{sec}^{-2}\text{volt}^{-1}$ ).

Use this method to determine a numerical estimate of  $e/m$ , and then show that in a 1 Tesla field  $|\omega_B| \approx 1.76 \times 10^{11}$  rad/sec. What is  $|\omega_B/\omega_0|$ , where  $\omega_0$  is the angular frequency of the 626.6 nm spectral line of neon? Is the criterion  $|\omega_B| \ll \omega_0$  of Problem 2(b) satisfied?

4. Given the results of Problems 2 and 3, and keeping terms to first order in  $\omega_B/\omega_0$ , show that

$$\left| \frac{\Delta\lambda}{\lambda_0} \right| = \frac{1}{2} \left| \frac{\omega_B}{\omega_0} \right| \quad (27.13)$$

where  $\lambda_0$  is the wavelength corresponding to  $\omega_0$ . Calculate the expected wavelength shift  $\pm\Delta\lambda$  of the neon 626.6 nm spectral line produced by a 1 Tesla field. How does this shift compare to the approximately  $8\text{\AA}$  width of the spectral lines shown in Figure 1?

5. Using equations (27.12) (on page 12) and (27.13), the definition  $\omega_B \equiv (e/m)B$ , and the separation  $d$  of the etalon mirrors, derive an equation relating the magnetic field strength  $B$  to  $|\Delta m|$  for the observed fringe splitting (as illustrated in Figure 8). Your equation should be independent of the wavelength  $\lambda_0$  (and  $\omega_0$ ). If  $d = 13.2$  mm, and using your answers to the previous problems, what is the required  $B$  to produce a Zeeman splitting of order  $\Delta m = 1$ ?

**You will need the equation you derive in this last problem to analyze the data you collect during the experiment! Make sure you get it right!**

**REFERENCES**

- Feynman, R., Leighton, R., & Sands, M. (1964, 2006). *The Feynman Lectures on Physics* (Vol. 1). Addison Wesley . Retrieved from <http://www.feynmanlectures.caltech.edu/>
- Kox, A. J. (1997). The discovery of the electron: II. The Zeeman effect. *European Journal of Physics*, 18(3), 139-144. Retrieved from <http://stacks.iop.org/0143-0807/18/i=3/a=003>
- Leighton, R. B. (1959). *Principles of Modern Physics*. New York: McGraw-Hill. Retrieved from <https://archive.org/details/PrinciplesOfModernPhysics>
- Martin, W. C., & Wiese, W. L. (2007). *Atomic Spectroscopy*. Retrieved from NIST Physical Measurement Laboratory: <http://www.nist.gov/pml/pubs/atSpec/index.cfm>
- Mulligan, J. F. (1997). Who were Fabry and Pérot? *American Journal of Physics*, 66, 797-802. doi:10.1119/1.18960
- Odom, B., Hanneke, D., D'Urso, B., & Gabrielse, G. (2006). New measurement of the electron magnetic moment using a one-electron quantum cyclotron. *Physical Review Letters*, 97. doi:10.1103/PhysRevLett.97.030801
- Pinnington, E. H. (1967). Accurate g-values for neon. *Journal of the Optical Society of America*, 57, 271-272. doi:10.1364/JOSA.57.0271\_1
- Racah, G. (1942). On a New Type of Vector Coupling in Complex Spectra. *Physical Review*, 61, 537. doi:10.1103/PhysRev.61.537



## APPENDIX A: QUANTUM THEORY OF ZEEMAN SPLITTING

The actual splitting of most atomic spectral lines in response to an applied magnetic field does not follow the classical, Lorentz-Zeeman theory. Observed splitting of the spectral lines of neon can be into from 2 to 9 lines each; only the two lines at 626.65nm and 585.25nm (wavelengths in air) behave as predicted. In this appendix we very briefly summarize the consequences of the modern, quantum-mechanical theory of atomic structure which can correctly describe the *anomalous Zeeman splitting* exhibited by the majority of neon's spectral lines.

### *Angular momentum and magnetic moment of a single atomic electron*

The Coulomb field of the nucleus forms, to an excellent approximation, a *central potential* well within which one or more electrons can be bound. As in the classical case, the total quantum-mechanical angular momentum of an isolated atom is a constant of the motion, and thus its angular momentum eigenstates may also be chosen to be eigenstates of the Hamiltonian (energy) operator  $\mathbf{H}$  (i.e., *stationary states*). Consider first a single electron bound to the atom's nucleus. The total angular momentum  $\vec{j}$  of the electron is the vector sum of two parts: its *orbital* angular momentum  $\vec{l} = \vec{r} \times \vec{p}$ , which is determined by the electron's spatial state (i.e. wave-function), and its intrinsic *spin* angular momentum  $\vec{s}$  (which is an inherent, quantum-mechanical property of the electron that has no classical analog).<sup>9</sup> Thus, for any particular single-electron state  $\vec{j} = \vec{l} + \vec{s}$ .<sup>10</sup>

Because the three Cartesian components of any quantum-mechanical angular momentum operator  $\vec{\mathbf{J}}$  do not commute, the complete, 3-dimensional angular momentum vector cannot be defined for any quantum state. States can be found, however, which are simultaneously eigenstates of the (squared) magnitude of the angular momentum operator,  $\mathbf{J}^2 = \vec{\mathbf{J}} \cdot \vec{\mathbf{J}}$ , and one Cartesian component (conventionally, the *z*-component),  $\mathbf{J}_z$ . In the case of a single electron, its *orbital angular momentum eigenstates*  $|\alpha; ll_z\rangle$  are characterized by two angular momentum quantum numbers  $l$  and  $l_z$  such that

$$\begin{aligned} \mathbf{L}^2 |\alpha; ll_z\rangle &= \hbar^2 l(l+1) |\alpha; ll_z\rangle; & l \in \{0, 1, 2, \dots\} \\ \mathbf{L}_z |\alpha; ll_z\rangle &= \hbar l_z |\alpha; ll_z\rangle; & l_z \in \{-l, -l+1, \dots, l-1, l\} \end{aligned} \quad (27.A.1)$$

---

<sup>9</sup> The discovery of electron spin involved many physicists during the 1920's. Although demonstrated experimentally by the Germans Otto Stern and Walther Gerlach in 1922, their results were misinterpreted. The Dutch physicists Uhlenbeck and Goudsmit and the Austrian-Swiss Wolfgang Pauli are generally credited with the first successful theory of the effects of electron spin on atomic structure.

<sup>10</sup> We use lower-case letters  $j$ ,  $l$ , and  $s$  to represent the total, orbital, and spin angular momenta of a single atomic electron state. Upper-case letters  $J$ ,  $L$ , and  $S$  are used for the net resulting angular momenta of an assemblage of atomic electrons. Bold, upper-case characters are used for the corresponding quantum-mechanical operators.

The extra  $\alpha$  in the state's *ket vector*  $|\alpha; ll_z\rangle$  represents all the other quantum numbers required to uniquely define that state.<sup>11</sup>

The electron's intrinsic spin angular momentum is characterized by the permanently-fixed quantum number  $s=1/2$ , making the electron a *fermion* subject to the *Pauli Exclusion Principle*: no two electrons may occupy identical quantum states. The  $z$ -component of the electron's spin angular momentum has a quantum number which may take on only two values:  $s_z = \pm 1/2$ . Because the electron's spin represents an independent degree of freedom, its eigenstates can be chosen to be simultaneously eigenstates of its orbital angular momentum, so a single-electron state vector, including spin, can be written as  $|\alpha; ll_z s_z\rangle$ . Any particular single-electron quantum state may be expanded as a linear combination (or *coherent superposition*) of the complete set of  $|\alpha; ll_z s_z\rangle$  for all the various allowed values of the quantum numbers.

Because the electron carries electrical charge  $-e$ , its orbital and spin angular momenta generate magnetic dipole moment vectors which add to produce an electron state's total magnetic moment  $\vec{m}$ . A magnetic dipole moment is associated with the orbital angular momentum of the single-electron state  $|\alpha; ll_z s_z\rangle$  because the orbiting charge of the electron creates a tiny current loop, thus producing a magnetic dipole field. Therefore the magnetic moment quantum vector operator  $\vec{M}$  is proportional to the orbital angular momentum operator:  $\vec{M} = -\mu_B \vec{L}$ .  $\mu_B$  is called the *Bohr magneton* and has a value of approximately  $5.79 \times 10^{-5}$  eV/Tesla; its expression in terms of fundamental constants is shown in (27.A.2). The minus sign arises because the electron has a negative charge. Since  $\vec{M}$  and  $\vec{L}$  are parallel, the  $z$ -component magnetic moment operator  $M_z$  is proportional to  $L_z$ , which has eigenvalue  $l_z$  for an electron in the state  $|\alpha; ll_z s_z\rangle$ . Therefore

$$\mathbf{M}_z |\alpha; ll_z s_z\rangle = -\mu_B \mathbf{L}_z |\alpha; ll_z s_z\rangle = -\mu_B l_z |\alpha; ll_z s_z\rangle; \quad \mu_B \equiv \frac{e\hbar}{2m_e} \quad (27.A.2)$$

Ignoring the effects of the electron's spin for a moment, the presence of an externally applied magnetic field will shift the  $|\alpha; ll_z\rangle$  state's energy by the potential energy of this dipole with respect to the field:<sup>12</sup>

$$\langle E_B \rangle = -\langle \alpha; ll_z | \vec{M} \cdot \vec{B} | \alpha; ll_z \rangle = \mu_B l_z B \quad (27.A.3)$$

---

<sup>11</sup> The concept of the *state vector* was integral to the *matrix mechanics theory* of quantum phenomena, first conceived by the German physicist Werner Heisenberg and later formulated by him and his colleagues Max Born and E. Pascual Jordan in a series of seminal papers in 1925; Heisenberg was awarded the 1932 Nobel Prize "for the creation of quantum mechanics." The British physicist Paul Dirac introduced the modern *bra* and *ket* notations for quantum state vectors, as well as the *Dirac delta function*  $\delta(\vec{r})$  and the notation  $\hbar$  for  $h/2\pi$ . We shall have more to say about Dirac later.

<sup>12</sup> This is strictly true only if  $E_B \ll \Delta E_0$ , where  $\Delta E_0$  is the energy difference to the next closest state. The formula presented in (27.A.3) is a result of the application of *first order perturbation theory* to estimate effect of the operator  $(-\vec{M} \cdot \vec{B})$  on the energy of a state.

The direction of the magnetic flux density  $\vec{B}$  determines the “z-axis” for the single, specifiable component of the state’s orbital angular momentum (with quantum number  $l_z$ ). Thus the presence of the magnetic field can *break the degeneracy* of the  $2l+1$  states  $|\alpha; ll_z\rangle$  sharing the quantum number  $l$  (for  $l > 0$ ), generating energy shifts of  $\mu_B B l_z$ , one for each allowed value of  $l_z$ .

The electron’s spin also generates a magnetic dipole moment, but in a different, purely quantum-mechanical way: the electron’s intrinsic magnetic moment cannot be identified with a physical circulation of charge (a current loop).<sup>13</sup> Again, the spin-induced dipole moment is proportional to the quantum-mechanical spin vector operator  $\vec{S}$ , but *the constant of proportionality is different*:  $\vec{M} = -g_e \mu_B \vec{S} \rightarrow \mathbf{M}_z |\alpha; l=0, l_z=0, s_z\rangle = -g_e \mu_B s_z |\alpha; 00s_z\rangle$ , where  $g_e$  is *the gyromagnetic ratio of the electron*. The most straightforward theory of the interaction of an  $s=1/2$  electron with an external electromagnetic field requires that  $g_e=2$ , and this value implies that the electron may have  $M_z = \pm \mu_B$ .<sup>14</sup> An early calculation based on the current, more modern and comprehensive theory of the interaction between electrons and the electromagnetic field (*quantum electrodynamics*, or QED) predicted that  $g_e/2=1.0011614$ , about a 0.1% correction.<sup>15</sup> Since an electron’s orbital and spin angular momentum vectors need not be parallel, and magnetic moment due to spin is different from that due to orbital angular momentum, the total magnetic moment they generate and the resulting energy shift  $\langle E_B \rangle = -\langle \vec{M} \cdot \vec{B} \rangle$  are not necessarily simple to calculate.

### ***Multiple-electron atoms; g-factor***

An atom with  $n$  electrons has a total angular momentum  $\vec{J} = \vec{L} + \vec{S}$ , where  $\vec{L}$  and  $\vec{S}$  are vector sums of the  $n$  electrons’ respective individual orbital and spin momenta  $\vec{l}$  and  $\vec{s}$ . Because the relative orientations of the individual electrons’ vector momenta can assume a variety of

---

<sup>13</sup> “Spin” cannot be caused by something physically “going around,” because  $\vec{r} \times \vec{p}$  angular momentum must have quantum numbers which are *integers* (any convenient quantum mechanics text should derive this result).

<sup>14</sup> Paul Dirac developed the first comprehensive, relativistically-correct quantum theory of the electron and its interaction with the electromagnetic field in an historic, then-controversial paper of 1928. In the course of his investigations he postulated that not only should the spin-1/2 electron have  $g_e=2$ , but that it must also be accompanied by what would later be interpreted as a companion *antiparticle*. Most relevant for our purposes, he used his theory to explain the anomalous Zeeman Effect in every detail. Dirac shared the 1933 Nobel Prize with Erwin Schrödinger. The *positron* (anti-electron) was identified by the Caltech physicist Carl Anderson in 1932, earning him the 1936 Nobel Prize.

<sup>15</sup> This value calculated by the American physicist Julian Schwinger in 1948 is engraved on his tombstone; Schwinger shared the 1965 Nobel Prize with Feynman and the Japanese physicist Sin-Itiro Tomonaga for their development of modern QED. For many years, refinements in the predicted value of  $g_e$  represented the most precise theoretical calculations of a fundamental physical constant, more precise than even the most accurate experimental measurements. This changed in 2006, with an experimental measurement by a team at Harvard (Odom, Hanneke, D’Urso, & Gabrielse, 2006) which included a Caltech alumnus (D’Urso) who, as an undergraduate, added the polarizer to our experiment’s apparatus. Current QED calculations and experimental measurements have precisions  $\sim 10^{-12}$ .

arrangements, the magnitudes of  $\vec{L}$  and  $\vec{S}$  can generally take on many possible values, even for a fixed set of  $n$  quantum numbers  $l$  for the electrons (they each, of course, have  $s=1/2$ ). The total  $\vec{L}$  and  $\vec{S}$  are, of course, angular momenta, and eigenstates of the squared magnitude operators  $\mathbf{L}^2$  and  $\mathbf{S}^2$  may be found with eigenvalues  $\hbar^2 L(L+1)$  and  $\hbar^2 S(S+1)$ , respectively, with quantum numbers  $L$  and  $S$ . The quantum number  $L$  for the total orbital angular momentum must be a nonnegative integer. The quantum number  $S$  for the total spin angular momentum must be a nonnegative integer if the number of electrons  $n$  is even;  $S$  is half-integer for  $n$  odd (e.g.  $\frac{1}{2}$ ,  $\frac{3}{2}$ , etc.). The total resultant angular momentum  $\vec{J}$  is similarly quantized, with  $\mathbf{J}^2$  and  $\mathbf{J}_z$  having eigenvalues  $\hbar^2 J(J+1)$  and  $\hbar J_z$  associated with quantum numbers  $J$  and  $J_z$ . In terms of  $L$  and  $S$ , The range of possible values for the quantum numbers  $J$  and  $J_z$  are

$$\begin{aligned} J &\in \{|L-S|, |L-S|+1, \dots, L+S-1, L+S\} \\ J_z &\in \{-J, -J+1, \dots, J-1, J\} \end{aligned} \quad (27.A.4)$$

(Note that if  $S$  is half-integer, then so will be  $J$  and  $J_z$ .) These relations are generally satisfied for the addition of any two angular momenta, not just  $L$  and  $S$ . For example, two electrons, both in states with  $l=1$ , may have a total, combined orbital angular momentum quantum number of  $L=1-1=0$ , or  $L=1$ , or  $L=1+1=2$ . Their total spin angular momentum quantum number may be either  $S=\frac{1}{2}+\frac{1}{2}=1$  or  $S=\frac{1}{2}-\frac{1}{2}=0$ . Using (27.A.4), the possible values for the total angular momentum quantum number  $J$  are then:

	$L=0$	$L=1$	$L=2$
$S=0$	$J=0$	$J=1$	$J=2$
$S=1$	$J=1$	$J=0$ or $J=1$ or $J=2$	$J=1$ or $J=2$ or $J=3$

Clearly in many cases a given amount of total angular momentum  $J$  might be obtained by combining different amounts of total orbital and spin angular momenta  $L$  and  $S$ , even from a set of atomic electrons with fixed values for their individual orbital angular momentum quantum numbers  $l$ . Upon examination of the above table, two electrons, each with  $l=1$ , could have  $J=1$  in the multi-electron eigenstates  $|JLS\rangle = |101\rangle$  or  $|110\rangle$  or  $|111\rangle$  or  $|121\rangle$ . In general, we should expect that such a two-electron atomic state with  $J=1$  would arise from some coherent superposition (mixture) of these four  $|1LS\rangle$  orthogonal eigenstates.

It may turn out, though, that a given  $J$  arises in a particular multi-electron atomic state from a single, pure  $|JLS\rangle$  state. Thus the multi-electron state is an eigenstate of both  $\mathbf{L}^2$  and  $\mathbf{S}^2$  as well as  $\mathbf{J}^2$  (rather than a coherent superposition of several such states as mentioned in the last paragraph). Such a state is said to be *LS* or *Russell-Saunders* coupled.<sup>16</sup> These  $|JLS\rangle$  states are

<sup>16</sup> Herbert. N. Russell was a very influential American astronomer of the early 20<sup>th</sup> century. Frederick A. Saunders was an accomplished American physicist who made important contributions to atomic spectroscopy. They described their angular momentum coupling scheme in a paper published in 1925.

particularly well suited for the calculation of energy shifts due to an externally-applied magnetic field, as we now show.

In general, for small values of the magnitude of an externally applied magnetic field  $\vec{B}$  oriented along the  $z$ -axis, eigenstates of  $\mathbf{J}^2$  and  $\mathbf{J}_z$  will experience proportional energy shifts of

$$\langle E_B \rangle = -\langle \vec{M} \cdot \vec{B} \rangle = g \mu_B J_z B \quad (27.A.5)$$

For atomic states with a given quantum number  $J$ , the coefficient  $g$  is independent of  $J_z$  and is called the atomic state's *g-factor*. Thus the energy shift of the state is proportional to  $J_z$ . Since the orientation of the  $z$ -axis is arbitrary, then as far as eigenstates of  $\mathbf{J}^2$  and  $\mathbf{J}_z$  are concerned, the atom's total magnetic moment vector  $\vec{M}$  *must be parallel to and proportional to* its total angular momentum vector  $\vec{J}$ . However,  $\vec{J} = \vec{L} + \vec{S}$ , whereas we would expect that the magnetic moment vector  $\vec{M} \propto \vec{L} + g_e \vec{S} = \vec{J} + (g_e - 1)\vec{S}$ . This vector  $\vec{M}$  would generally not be parallel to  $\vec{J}$ . The quantum-mechanical resolution to this conundrum is to require that the quantum operator  $\vec{M}$  *be proportional to the projection of this latter vector onto the direction of  $\vec{J}$* :<sup>17</sup>

$$\vec{M} \propto \vec{J} \left[ 1 + (g_e - 1) \frac{\vec{J} \cdot \vec{S}}{\mathbf{J}^2} \right] \quad (27.A.6)$$

We can find the value of  $\vec{J} \cdot \vec{S}$  as follows: since  $\vec{J} = \vec{L} + \vec{S}$ , then  $\vec{L} = \vec{J} - \vec{S}$  and

$$\begin{aligned} \mathbf{L}^2 &= (\vec{J} - \vec{S}) \cdot (\vec{J} - \vec{S}) = \mathbf{J}^2 + \mathbf{S}^2 - 2\vec{J} \cdot \vec{S} \\ \therefore 2\vec{J} \cdot \vec{S} &= \mathbf{J}^2 + \mathbf{S}^2 - \mathbf{L}^2 \end{aligned}$$

The *LS* coupled,  $|JLS\rangle$  states are eigenstates of the RHS of the above expression, so for these states (27.A.6) becomes

$$\vec{M} \propto \vec{J} \left[ 1 + (g_e - 1) \frac{J(J+1) + S(S+1) - L(L+1)}{2J(J+1)} \right]$$

Comparing this result to (27.A.5), we find that an *LS* coupled,  $|JLS\rangle$  state's *g-factor* is given by

$$g = 1 + (g_e - 1) \frac{J(J+1) + S(S+1) - L(L+1)}{2J(J+1)} \quad (27.A.7)$$

Setting  $g_e \equiv 2$  in (27.A.7) results in what is called the *Landé g-factor* for the *LS* coupled state.<sup>18</sup> Applying this result to the example we presented earlier (the  $J=1$  states of a two-electron system, each with orbital quantum number  $l=1$ ), possible values for the Landé *g-factor* are:  $|JLS\rangle = |101\rangle: g=2$ ;  $|110\rangle: g=1$ ;  $|111\rangle: g=3/2$ ;  $|121\rangle: g=1/2$ . In the case of a coherent

<sup>17</sup> Rigorously, the results presented here follow from the *Wigner-Eckart theorem*, part of the representation theory of *Lie groups* (physicists Eugene Wigner and Carl Eckart).

<sup>18</sup> The German physicist Alfred Landé published this result in 1921.

superposition of these states, the resultant  $g$ -factor to be used in equation (27.A.5) would be a weighted average of these four values.

### ***Spectroscopic term notation***

The individual electrons in an atom occupy stationary states with various values for each electron's angular momentum quantum numbers  $l$ ,  $l_z$ , and  $s_z$ . In addition, the principal quantum number  $n$  determines how deeply into the nuclear Coulomb potential well an electron state resides and determines the electron state's binding energy (except for usually relatively small corrections due to *spin-orbit coupling*, mutual electrostatic repulsion among the electrons, and several other effects). The principal quantum number  $n$  can assume only positive integer values, with  $n = 1$  representing the most strongly bound states (binding energy decreases with increasing  $n$  approximately as  $n^{-2}$ ).

For any particular  $n$ , the orbital angular momentum quantum number  $l$  is restricted to an integer value in the set  $l \in \{0, 1, \dots, n-1\}$ . Thus, for example,  $l$  must equal 0 in the  $n = 1$  states, but  $l$  can equal 0 or 1 in the  $n = 2$  states, etc. For any particular value of  $l$ , single electron states exist with  $l_z \in \{-l, -l+1, \dots, l-1, l\}$  and with  $s_z = \pm 1/2$ . Thus for a particular choice of  $n$  and  $l$ , there are a total of  $2(2l+1)$  single-electron states, and counting all allowable choices for  $l$ ,  $l_z$ , and  $s_z$ , there are a total of  $2n^2$  single-electron states with principal quantum number  $n$ . Because electrons are fermions, there can exist at most one electron occupying each of these states. The  $2n^2$  single-electron states with principal quantum number  $n$  collectively make up an atomic *shell*. The  $2(2l+1)$  single-electron states with a specified  $n$  and  $l$  make up a *subshell*. It can be shown that a completely filled atomic subshell holding  $2(2l+1)$  electrons will form a multi-electron state which is completely spherically-symmetric and therefore have total  $J = L = S = 0$ . This is then also true for any completely filled shell as well.

*Spectroscopic notation* denotes the orbital angular momentum quantum numbers of the various occupied atomic subshells using letter symbols from the following table:

$l$ value:	0	1	2	3	4	5	...
symbol:	$s$	$p$	$d$	$f$	$g$	$h$	...

A specific subshell is prefixed with its  $n$  value, as in:  $1s$ ,  $2s$ ,  $2p$ ,  $3s$ ,  $3p$ ,  $3d$ , etc. If more than one electron occupies a subshell, then the number of electrons is denoted by a superscript, e.g.  $2p^5$ . For example, the *electron configuration* of the ground state of neon is written as  $1s^2 2s^2 2p^6$ ; the ground state of sodium is  $1s^2 2s^2 2p^6 3s$ .

A *spectroscopic term* expression describes a multi-electron,  $LS$  coupled  $|JLS\rangle$  state using the following format:  $^{2S+1}L_J$ , where the *spin multiplicity* prefix is an integer (the number of possible values for  $S_z \in \{-S, -S+1, \dots, S-1, S\}$ ), the value for  $L$  is denoted by an upper-case version of the appropriate letter found in the previous table, and a number suffix (integer or half-integer) is used for the total angular momentum quantum number  $J$ . Thus  $^1S_0$  represents  $|000\rangle$ , the term

for any completely filled or empty subshell;  ${}^2P_{1/2}$  for  $|\frac{1}{2}1\frac{1}{2}\rangle$ ; etc. If the multi-electron state has *odd spatial parity*, i.e.  $\langle -\vec{r} | JLS \rangle = -\langle \vec{r} | JLS \rangle$ , then the term includes a trailing “o” as in  ${}^2P^o_{1/2}$ . For example, one particular singly-ionized, *LS* coupled state of neon could be described as:  $1s^22s^22p^5({}^2P^o_{3/2})$ , which, according to equation (27.A.7), would be expected to have a Landé *g*-factor of  $4/3$  ( $J = \frac{3}{2}$ ,  $L = 1$ ,  $S = \frac{1}{2}$ ).

### ***Racah’s *Jl* coupling scheme for excited atomic states***

One other common angular momentum coupling scheme should be mentioned, because it is particularly relevant to the theoretic analyses of the observed Zeeman splitting of the transitions in neon between the excited state configurations ( $1s^22s^22p^5$ )  $3p \rightarrow 3s$  and  $4d \rightarrow 3p$ , transitions which produce most of the bright spectral lines shown in Figure 1. This scheme, known as *Jl* coupling, combines the orbital angular momentum  $l$  of a lone excited electron with the total angular momentum  $J_{\text{core}}$  of the remaining *LS* coupled core electrons ( $1s^22s^22p^5$  for the neon lines we’re considering). The resulting combined angular momentum  $K$  would be chosen from the set of possibilities  $K \in \{|J_{\text{core}} - l|, \dots, (J_{\text{core}} + l) - 1, J_{\text{core}} + l\}$ . The excited electron’s spin  $s$  is then combined with  $K$  to give a final total  $J$  of  $|K \pm \frac{1}{2}|$ , as first described in (Racah, 1942).<sup>19</sup>

The accepted spectroscopic term notation used for a state defined by *Jl* coupling is, for example,  $1s^22s^22p^5({}^2P^o_{3/2})3p^2[5/2]_2$ , with  ${}^{2s+1}[K]_J$  as the term descriptor of the final, *Jl* coupled term, and the term describing the core electrons’ *LS* coupled state is listed in parenthesis. This is the notation used to describe neon’s atomic configurations on the NIST website (Martin & Wiese, 2007). The *g*-factor for *Jl* coupled states is given in (Racah, 1942) as ( $J_{\text{core}}$  and  $g_{\text{core}}$  are the total angular momentum and *g*-factor of the *LS* coupled state of the core electrons, and we use the simple approximation  $g_e = 2$ ):

$$g_{Jl} = \frac{2J+1}{2K+1} + 2(g_{\text{core}} - 1) \frac{K(K+1) + J_{\text{core}}(J_{\text{core}}+1) - l(l+1)}{(2K+1)(2J+1)} \quad (27.A.8)$$

For the neon example given above,  $1s^22s^22p^5({}^2P^o_{3/2})3p^2[5/2]_2$ , then  $J_{\text{core}} = 3/2$ ,  $g_{\text{core}} = 4/3$  (using equation (27.A.7)),  $l = 1$ ,  $K = 5/2$ , and  $J = 2$ . The resulting  $g = 16/15 \approx 1.067$ . The two other *Jl* coupled combinations which can also result in  $J = 2$  are:  $1s^22s^22p^5({}^2P^o_{3/2})3p^2[3/2]_2$  ( $g = 43/30 \approx 1.433$ ) or  $1s^22s^22p^5({}^2P^o_{1/2})3p^2[3/2]_2$  ( $g = 7/6$ ). In contrast, if we were to simply *LS* couple the complete  $1s^22s^22p^53p$  electron configuration (keeping in mind the limitations on the possible core electron states demanded by Pauli exclusion), the possible states with total  $J = 2$  then have terms of  ${}^3P_2$  ( $g = 3/2$ ),  ${}^3D_2$  ( $g = 7/6$ ), or  ${}^1D_2$  ( $g = 1$ ). The consequences of these various possibilities on the expected Zeeman splitting of the neon spectral lines are

---

<sup>19</sup> Giulio Racah was a mid-twentieth-century Italian-Israeli physicist who made several important contributions to the modern quantum theory of multi-electron atomic states and atomic spectroscopy.

analyzed in a later section. Of course, any  $Jl$  coupled state may be expressed as a coherent superposition of  $LS$  coupled states.

### ***Electric dipole radiation selection rules and Zeeman splitting***

Visible light has wavelengths of  $\sim 400\text{--}800$  nm, thousands of times greater than an atomic diameter ( $\sim 1\text{--}3\text{\AA}$ ). Consequently, an electromagnetic wave in this wavelength range primarily affects an atom's electrons through oscillations of its electric field in the atom's vicinity. This oscillating field can exchange energy (in the form of photons) with the atom and cause transitions between atomic states whose energy difference  $\Delta E = \hbar\omega$ , where  $\omega$  is the angular frequency of the electric field oscillation. Such transitions correspond to the classical, electric dipole radiation discussed in the main text (pages 27-2 ff.), and are therefore known as *electric dipole* transitions. In fact, the analogy is more than just a casual resemblance to the classical situation. As you will learn in your quantum mechanics course, one can represent a perturbing force by an operator  $\mathbf{G}$  applied to the quantum state  $|\psi\rangle$  to generate the new state  $|\psi'\rangle = \mathbf{G}|\psi\rangle$ . The probability that this new state is observed to correspond to some specified state  $|\phi\rangle$  is given by the squared magnitude of the matrix element of  $\mathbf{G}$  connecting  $|\psi\rangle$  and  $|\phi\rangle$ :

$$|\langle\phi|\psi'\rangle|^2 = |\langle\phi|\mathbf{G}|\psi\rangle|^2$$

In the case of an oscillating electric field experienced by a single electron (such as the transverse electric field produced by a passing electromagnetic wave), the relevant operator is proportional to the dot product of the field's *polarization vector*  $\vec{E}$  and the electron's electric dipole moment vector  $-e\vec{\mathbf{R}}$  ( $\vec{\mathbf{R}}$  is the electron's *position operator*):  $\vec{E} \cdot e\vec{\mathbf{R}} = e(E_x\mathbf{X} + E_y\mathbf{Y} + E_z\mathbf{Z})$ . Thus to determine the probability of such a field leading to an observed transition between two single-electron spatial states  $|nll_z\rangle$  and  $|n'l'l'_z\rangle$ ,<sup>20</sup> we must evaluate the *matrix elements* of the three Cartesian position operators

$$\langle n'l'l'_z | \mathbf{X} | nll_z \rangle, \quad \langle n'l'l'_z | \mathbf{Y} | nll_z \rangle, \quad \langle n'l'l'_z | \mathbf{Z} | nll_z \rangle$$

As shown in *Leighton* as well as in many elementary quantum mechanics texts, these matrix elements will all generally vanish unless the following electric dipole transition *selection rules* obtain ( $\Delta n = n' - n$  can be anything, including 0, as long as  $n > l$  and  $n' > l'$ ):

$$\begin{aligned} \mathbf{X}, \mathbf{Y}, \mathbf{Z}: \quad \Delta l = l' - l = \pm 1 \quad \text{and} \quad \Delta s_z = 0 \\ \mathbf{X}, \mathbf{Y}: \quad \Delta l_z = l'_z - l_z = \pm 1 \\ \mathbf{Z}: \quad \Delta l_z = 0 \end{aligned} \tag{27.A.9}$$

---

<sup>20</sup> We ignore the electron's spin quantum number  $s_z$  because the oscillating electric field of the passing visible-light photon has little effect on a magnetic dipole moment, and the photon's oscillating magnetic field is relatively insignificant because of the photon's long wavelength (low frequency). *Magnetic dipole* transitions can occur, however, but at a very low rate (and are thus known as a class of *forbidden transitions*).



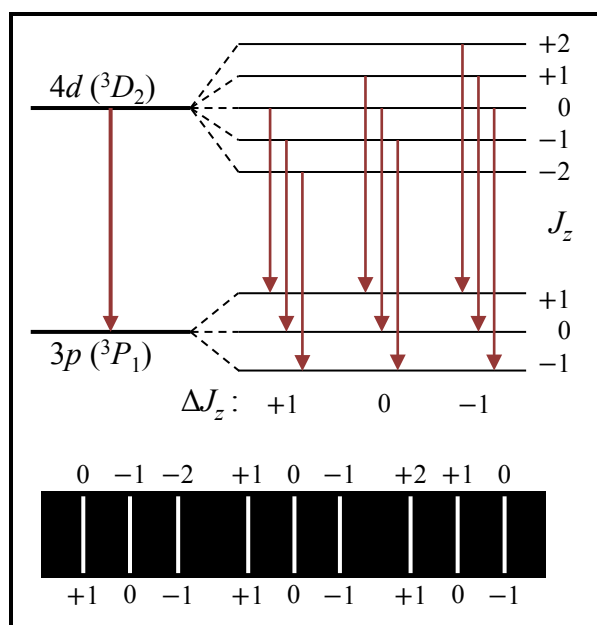
These electric dipole transition selection rules may be extended in a straightforward manner to  $LS$  coupled multi-electron states  $|JLS\rangle$ . The most basic requirements for an electric dipole transition is that only one electron changes its state, and this electron must have its  $\Delta l = \pm 1$  (for the case of  $Jl$  coupling, the lone excited electron transitions). Additionally, the electrons' combined spatial wave function must change parity. As for the atom as a whole,

$$\begin{aligned} \Delta J &= 0, \pm 1 & (J = 0 \rightarrow J = 0 \text{ forbidden}) \\ \Delta J_z &= 0, \pm 1 & (J_z = 0 \rightarrow J_z = 0 \text{ forbidden if } \Delta J = 0) \\ \Delta L &= 0, \pm 1 & (L = 0 \rightarrow L = 0 \text{ forbidden}) \\ \Delta S &= 0 \end{aligned} \tag{27.A.10}$$

Justification for the rules may be found in *Leighton*. The relationship between the polarization of the emitted radiation and  $\Delta J_z$  is the same as that for  $\Delta l_z$  in (27.A.9): for linear polarization purely in a plane containing the  $z$ -axis,  $\langle J' L' S J_z' | \mathbf{Z} | J L S J_z \rangle$  is non-vanishing, and  $\Delta J_z = 0$ ; if  $\Delta J_z \neq 0$ , then the polarization is generally elliptical with a non-vanishing component perpendicular to the  $z$ -axis.

Now consider an electric dipole transition in the presence of an applied magnetic field aligned with the  $z$ -axis. The field will shift the energies of states having different  $J_z$  in accordance with equation (27.A.5):  $\langle E_B \rangle = -\langle \vec{\mathbf{M}} \cdot \vec{\mathbf{B}} \rangle = g \mu_B J_z B$ . Assume that a single electron transitions from  $4d$  to  $3p$ , with initial and final  $LS$  coupled states  $|JLS\rangle_i = |221\rangle$  (or  ${}^3D_2$ ) and  $|JLS\rangle_f = |111\rangle$  (or  ${}^3P_1$ ). The electric dipole selection rules listed above are satisfied, and equation (27.A.7) gives  $g$ -factors of  $g_i = 7/6$  and  $g_f = 3/2$ . The resulting allowable state transitions are shown in Figure 12.

**Figure 12: An example of Zeeman splitting of a hypothetical electric dipole transition of a single electron ( $4d \rightarrow 3p$ ). The term symbols of the initial and final  $LS$  coupled states are also shown. Applying a magnetic field splits the energy degeneracy of the various initial and final  $J_z$  states (the splitting is greatly exaggerated). The selection rules in (27.A.10) allow 9 different transitions; each has a different energy  $\Delta E_B$  because the initial and final states'  $g$ -factors differ (see text). A diagram showing the relative locations of the 9 resulting spectral lines is also shown, along with each line's initial and final  $J_z$ .**



If the two states'  $g$ -factors were the same, then the application of a magnetic field would split the spectral line into only three distinct wavelengths, rather than the nine shown in Figure 12. Only if both  $g$ -factors = 1, would the splitting match the normal Zeeman Effect predicted by Lorentz (or one of the states has  $J = 0$  and the other has  $J = 1$  and  $g = 1$ ).

### *Normal Zeeman lines of neon*

Now consider the two prominent normal Zeeman lines in the neon spectrum at wavelengths of 585.2nm and 626.6nm. Each line is generated by a transition between the configurations  $1s^2 2s^2 2p^5 3p \rightarrow 1s^2 2s^2 2p^5 3s$ . For each of these lines, both the initial and final states have 9 core electrons ( $1s^2 2s^2 2p^5$ ) combined via  $LS$ -coupling to give the odd-parity term  ${}^2P^\circ_{1/2}$  ( $J = 1/2$ ,  $L = 1$ ,  $S = 1/2$ ). The excited electron's orbital and spin angular momenta may assume different orientations relative to the  $\vec{J}$ ,  $\vec{L}$ , and  $\vec{S}$  of the core, resulting in the energy difference between the transitions generating the two spectral lines.

In the case of the 585.2nm spectral line, the excited,  $n = 3$  electron combines with the core electrons to form the overall nearly pure  $LS$  coupled terms  $1s^2 2s^2 2p^5 ({}^2P^\circ_{1/2}) 3p {}^1S_0 \rightarrow 1s^2 2s^2 2p^5 ({}^2P^\circ_{1/2}) 3s {}^1P^\circ_1$  (i.e.,  $|000\rangle \rightarrow |110\rangle$ ). In both states the excited electron's spin combines with the five  $2p$  electrons' spins to give an overall net  $S = 0$ . In its initial  $3p$  state the excited electron's orbital angular momentum cancels that of the core, giving a total net  $J = L = S = 0$ : the overall angular momentum of the atom's six  $p$  electrons ( $2p^5 3p$ ) is the same as that of its filled, ground state configuration ( $2p^6$ ). Since the excited electron's spin does not change orientation during its electric dipole transition to  $3s$ , the total spin  $S$  of the atom's electrons remains 0, while the loss of the excited electron's orbital angular momentum ( $\Delta l = -1$ ) leaves a net  $L = 1$  for the atom's total orbital angular momentum. Thus  $J = 0$  in the initial state, and  $J = 1$  and  $g = 1$  in the final state, making this transition a good example of the quantum analog to Lorentz's theory. The experimentally determined  $g$ -factor of the 585.2nm final state is  $1.037 \pm 0.002$ , only 4% away from the pure  $LS$  coupled  ${}^1P^\circ_1$  state Landé value.<sup>21</sup>

In the 626.6nm normal Zeeman transition, on the other hand, it is the initial state which has net angular momentum. As in the previous case, the  $3p$  electron's spin cancels that of the core electrons to give an overall net  $S = 0$ . The  $L = 1$  orbital angular momentum of the core's  ${}^2P^\circ_{1/2}$  term combines with the  $3p$  electron's  $l = 1$  to yield  $J = L = 1$  for the atom's total orbital angular momentum. Thus the initial state term is the very nearly pure,  $LS$  coupled  $1s^2 2s^2 2p^5 ({}^2P^\circ_{1/2}) 3p {}^1P_1$  ( $|110\rangle$ ). Following the excited electron's transition to  $3s$ , however, it assumes the  $JL$  coupled state  $1s^2 2s^2 2p^5 ({}^2P^\circ_{1/2}) 3s {}^2[1/2]^\circ_0$ , in which its spin combines with that of the core's total angular momentum of  $1/2$  to yield  $J = 0$ . The measured  $g$ -factor of the 626.6nm initial state is  $0.994 \pm 0.004$ .

---

<sup>21</sup> Measured  $g$ -factors are from (Pinnington, 1967).